

This work was written as part of one of the author's official duties as an Employee of the United States Government and is therefore a work of the United States Government. In accordance with 17 U.S.C. 105, no copyright protection is available for such works under U.S. Law.

Public Domain Mark 1.0

<https://creativecommons.org/publicdomain/mark/1.0/>

Access to this work was provided by the University of Maryland, Baltimore County (UMBC) ScholarWorks@UMBC digital repository on the Maryland Shared Open Access (MD-SOAR) platform.

Please provide feedback

Please support the ScholarWorks@UMBC repository by emailing scholarworks-group@umbc.edu and telling us what having access to this work means to you and why it's important to you. Thank you.

PROCEEDINGS OF SPIE

SPIDigitalLibrary.org/conference-proceedings-of-spie

Focusless hand-held proximal Raman detection and two-dimensional mapping of explosives

Eric Languirand, G. Amalthea Trobare

Eric R. Languirand, G. Amalthea Trobare, "Focusless hand-held proximal Raman detection and two-dimensional mapping of explosives," Proc. SPIE 12541, Chemical, Biological, Radiological, Nuclear, and Explosives (CBRNE) Sensing XXIV, 125410A (14 June 2023); doi: 10.1117/12.2662856

SPIE.

Event: SPIE Defense + Commercial Sensing, 2023, Orlando, Florida, United States

Focus-less hand-held proximal Raman detection and two-dimensional mapping of explosives

Eric R. Languirand^{*a}, G. Amalthea Trobare^b

^a US Army DEVCOM CBC, 8510 Ricketts Point Rd. Gunpowder, MD 21010; ^b University of Maryland Baltimore County, 1000 Hilltop Circle, Baltimore, MD USA 21250

ABSTRACT

Raman sensing and mapping techniques traditionally use a tightly focused laser beam to incite and collect Raman scattered photons. A large amount of energy is typically focused in a very small (micron-sized) area potentially resulting in photo-induced damage and can be not eye-safe. In addition, when using a focused-based laser system, scanning a large area is time consuming due to the small area of interrogation and must be done at a specific distance. Therefore, either prior knowledge of the sample location (in three dimensions) is necessary, or a smaller area must be scanned.

In this work, we demonstrate a hand-held proximal Raman detection instrument that uses a non-focused laser beam to interrogate a larger area. This reduces the time it takes to map a surface and provides greater flexibility in targeting the area to interrogate. Herein, we show detection and mapping of explosives in two dimensions with this hand-held proximal Raman instrument as well distance dependence of this non-focused instrument with explosive materials.

Keywords: Raman, Proximal, Standoff, non-focused, collimated, explosives, mapping

1. INTRODUCTION

Raman scatter inherently has a weak cross section and as such, traditional Raman measurements tightly focus a laser light onto an area of interest to maximize the photons per unit area.¹ The vibrational movements of a molecule that the laser light interacts with and provides Raman scatter from can help realize chemical identification.^{2,3} The benefits of chemical characterization coupled with the tightly focused laser beam often requires the instrument to be in close contact with the analyte/sample. Alternatively, stand-off techniques can provide a distance of 200m from the instrument (and therefore user), but still requires precise placement of the sample within the focal region of the telescopic lens.⁴⁻⁷ Increasing flexibility in distancing typically results in the use of adjustable or automated optics, distance ranging, or other clever techniques but when employed, will increase at least one of the following: size, weight, power, or cost (SWaP-C).

To mitigate increases in SWaP-C, utilizing collimated laser light to induce Raman scatter from a surface has been recently developed in a lab-based free-space optical arrangement.⁸ In this arrangement, a collimated laser beam interrogates a sample at an arbitrary distance away and collects the 180° backscatter light via a collimated optic that is located at the instrument location.⁸ There are no focusing optics used, and only collimated light is sent to the sample and collimated light is received by the spectrometer resulting in nearly steady Raman signal out to 10m.

This work evaluates the lab-based free-space optical technique that has been reduced to a hand-held proximal Raman detector. The free-space optics were replaced with optical fibers and provided laser light that is not focused to interrogate an analyte. The hand-held instrument evaluates explosive-based materials at distances out to 12m as well as an application of imaging with the handheld instrument.

2. METHODS

2.1 Instrumentation

The instrumentation used in this work for collecting Raman spectra is a handheld proximal Raman detector that is approximately 2.5L in volume with a form factor that is similar to a battery-operated drill. The system weighs 4.6lbs with a 12V, 4.0Ah standard battery and consists of a CW 785nm diode laser and spectrometer. The proximal Raman detector had two sets of optical configurations that could be used: one in which the optical beam was controlled with 8mm collimating optics and another in which the optical beam was controlled with 50mm collimating optics. The instrument

was controlled via a touch screen integrated into it. High resolution images were obtained using a digital microscope (Keyence VHX-7000). All spectral data and image data was processed using MATLAB R2021b (Mathworks, USA).

2.2 Chemical and Distance Analysis

Ammonium nitrate ($\geq 98\%$), potassium chlorate ($\geq 99\%$), and naphthalene (99%) were purchased from Sigma-Aldrich and were used as received without any additional purification. Small quantities of HMX, RDX, C4, and ammonium nitrate mixed with fuel oil (ANFO) were acquired from different branches at the Chemical Biological Center and were used as received without any additional purification. Each trial consisted of at least 45 seconds of spectral acquisition which results in at least 9 spectra obtained. Each trial was done in at least triplicate, unless otherwise noted.

Laser beam diameters can be measured by physically measuring the diameter of the beam at different distances.^{9, 10} For the two optical configurations laser beam diameters were determined by capturing a digital image (Nikon Digital Camera D7200) of the laser that was impinging on a white piece of copy paper that had a scale present within the imaging area (American Board of Forensic Odontology (ABFO) No. 2). A custom MATLAB script was used to analyze a region of interest across the scale bar whereby the intensity of the selected region was summed to obtain a two-dimensional representation of the pixels which resulted in a signal that appeared to be wave-like in intensity across the demarcations of the ruler. Next, Fast Fourier Transform (FFT) was performed on that region resulting in a frequency of the demarcations on the ruler in pixel/mm units resulting in a completely objective method for measuring the scale of the images.

The beam diameters were measured via ImageJ (1.53a, National Institutes of Health, USA) whereby an area of the digital image was selected, converted to 8-bit gray scale, and a threshold was determined via the Otsu method¹¹ in order to isolate the laser spot on the copy paper. A circle was drawn encompassing the laser spot and beam diameters were determined from that.

Distance dependence analysis was completed using ammonium nitrate that was spread into a large petri dish (6" diameter), packed solid, and sealed with parafilm to create a packed, homogenous surface to obtain the ammonium nitrate spectrum from. Spectra were obtained at various distances out to approximately 12m.

2.3 Raman Imaging

Various amounts of ammonium nitrate were placed on a 2" by 2" stainless steel coupon. Two independently controlled translational stages were mounted perpendicular to each other for x- and y-axis control. The stainless steel coupon was mounted within a plastic Petri dish which was then mounted onto the translational stages (for easy transport to and from the microscope for high resolution digital imaging). The Raman image was collected via raster scanning in 7mm increments across the coupon for a total of 64 (8x8) pixels. The instrument when configured with the 8mm optics was placed 0.16m from the stainless steel coupon (laser light was reflected down to the surface via a mirror) and when configured with the 50mm optics was placed 0.2m from the stainless steel coupon. Spectra were collected the same way as previously described. All data was processed in MATLAB R2021b via custom scripts.

3. RESULTS AND DISCUSSION

3.1 Spectral Results

The handheld proximal Raman detector obtains background corrected spectra that can be exported as CSV files. The instrument is able to collect backscattered Raman signal without a focusing lens thereby providing flexibility in where the user can position themselves when using the instrument. Figure 1 shows various spectra associated with explosives including precursors of potassium chlorate and ammonium nitrate as well as explosive materials of HMX, RDX, C4, and ammonium nitrate mixed with fuel oil (ANFO). Potassium chlorate shows the ν_1 symmetric stretching of the ClO_4^- ion with its strongest peak in the Raman spectrum at 936cm^{-1} (literature: 942cm^{-1}).⁶ Ammonium nitrate's symmetric stretch of NO_3^- is shown at 1041cm^{-1} (literature: 1044cm^{-1}).¹² In this work, potassium chlorate and ammonium nitrate are classified as precursors.

HMX, RDX, C4 and ANFO are considered high explosives. HMX is confirmed with the symmetric NC_2 and NO_2 vibrations at 840cm^{-1} and 1313cm^{-1} (literature: 838cm^{-1} and 1328cm^{-1}), respectively.¹² RDX presents a weak NN stretch with NO_2 axial scissoring and CH_2 twisting at 848cm^{-1} and 1388cm^{-1} (literature: 858cm^{-1} and 1378cm^{-1}), respectively.¹² C4 and RDX strongly agree with the same peaks as C4 is 90% RDX by weight.¹² ANFO provides a strong symmetric stretch of NO_3^- at 1041cm^{-1} consistent with what is seen for ammonium nitrate. This agreement is expected as ANFO is ammonium nitrate with fuel oil.¹³ The strong fluorescence in the spectrum is likely due to the addition of the fuel oil.

In addition to the spectral peaks noted here, there are other peaks that are consistently dominating the spectra of each compound. These peaks are present at ca 400cm^{-1} , 520cm^{-1} , 665cm^{-1} , 1336cm^{-1} , 1543cm^{-1} , and 2873cm^{-1} . These peaks are likely due to the room lighting despite processing with background subtraction. The spectra were not post-processed to remove the background by the author and the only additional processing was smoothing of the spectra via a one-dimensional median filter with an order of 15.

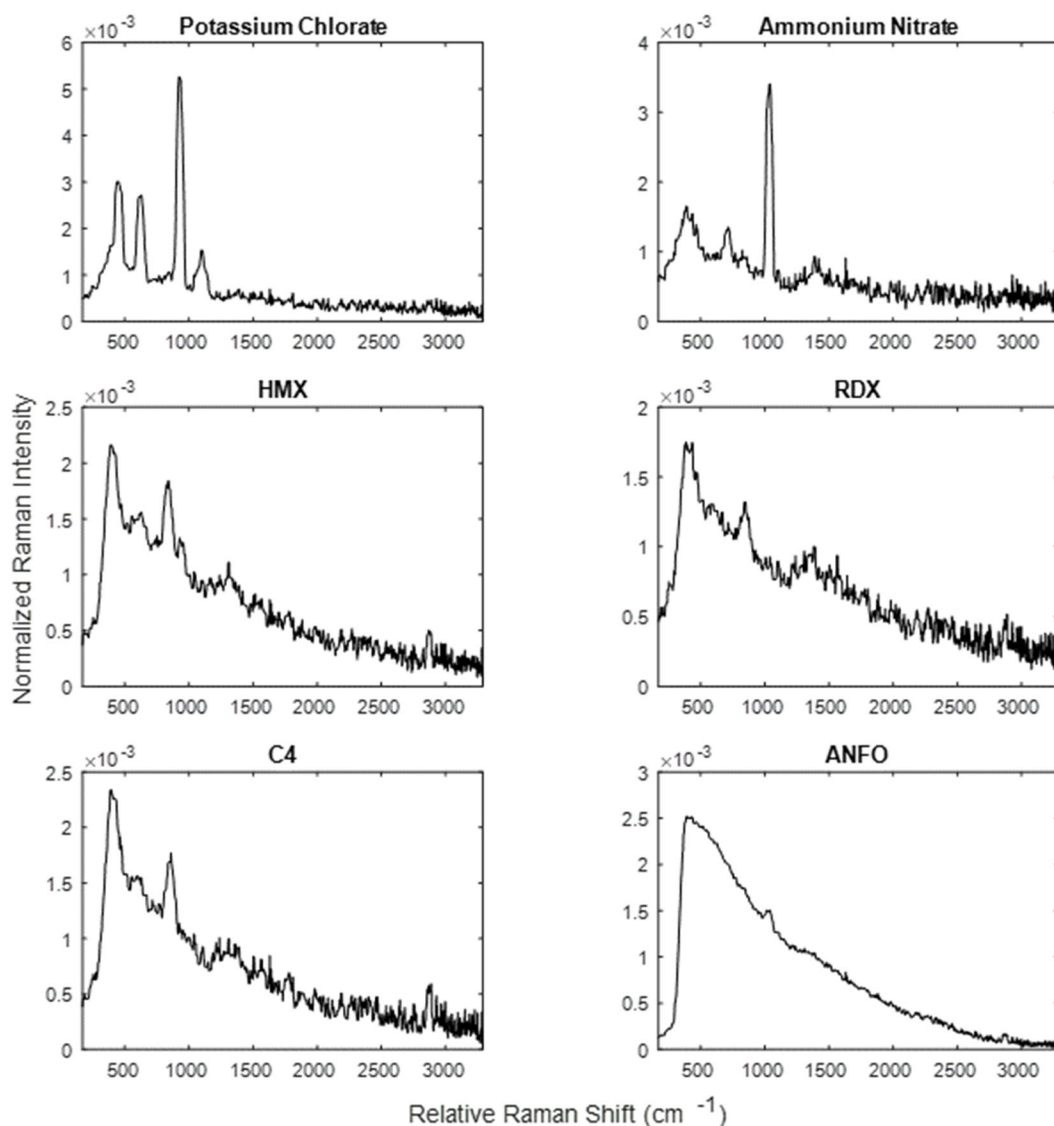


Figure 1: Raman spectra obtained with the proximal Raman detector approximately 0.3m away with no focusing optics. Spectra include precursors of potassium chlorate and ammonium nitrate and explosive materials of HMX, RDX, C4, and ANFO.

3.2 Distance Dependence of Raman Signal

In understanding how the Raman signal changes as a function of distance for a non-focusing system, it is first important to understand how collimated the laser is as this will drastically affect the performance. In contrast to a perfectly collimated system, recall how a tightly focused laser will have a shallow focal plane resulting in rapid signal loss as Raman scatter is collected outside of the focal plane.

The degree of collimation of the proximal Raman system was determined by calculating the divergence of the excitation beam (i.e. visible laser light). This is typically completed by looking at the beam waste of a Gaussian beam at 1/e of the maximum intensity.¹⁰ We modify this as we are not looking at a focused laser beam, but instead look at the width of the beam over several distances using image processing techniques. The illuminated area by the laser light was captured with a digital image and processed to determine the beam diameter at several distances. This was completed with two different optics resulting in two different areas that would be interrogated at the collection area and results in two different divergences. These results are shown in Figure 2. The 8mm optical configuration are diverging to a greater extent than the 50mm optical configuration, as can be determined from the slopes of the line:

$$\theta = \frac{(D_f - D_i)}{(l_f - l_i)} \quad (1)$$

Where θ is divergence D is the diameter of the of the excitation beam at the final (f) location compared to the initial (i) location and l is the length from the front of the instrument to the target at the final location compared to the initial location. The divergence is equivalent to the slope. Herein, the 8mm optical configuration diverge 9.1mm/m (diameter of beam/distance of target) and the 50mm optical configuration diverge 2.4mm/m. The 50mm optical configuration have a divergence that is approximately 3.8 times less than that of the 8mm optical configuration.

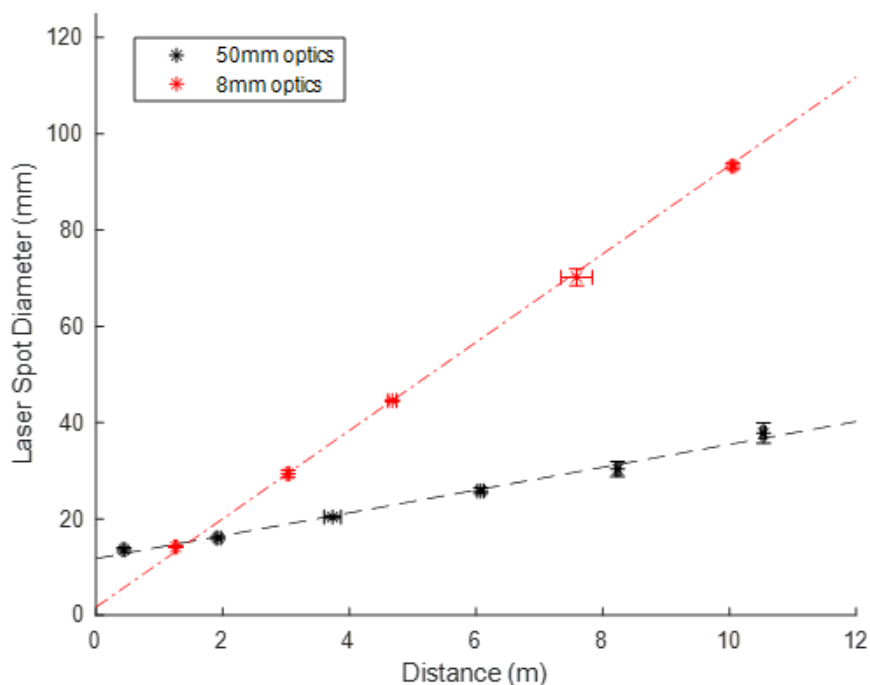


Figure 2: Divergence of the excitation laser light with 50mm optics (black data) and with 8mm optics (red data).

The degree of divergence effects the signal that is returned to the spectrometer. In this analysis, ammonium nitrate spread thickly over a 6-inch diameter surface and pressed for uniformity and was used to produce a homogenous sample to interrogate. The signal from the ammonia nitrate peak at 1041cm^{-1} was used in the distance dependence measurements, shown in Figure 3. The two configurations (8mm and 50mm optics) were fit to a double exponential. The fit to a single exponential was poor and did not incorporate the data well. However, the first exponential term appears to be dominating for the 8mm optics and the 50mm optics, with the second exponential term being only $< 1\%$ and approximately 2% of the first exponential term, respectively. As shown in Figure 3, the 8mm optical configuration decay at a rapid rate, resulting in a distance dependence of approximately $1/d^{1.9}$. The expected rate of decay in signal with a focusing lens would be $1/d^2$. While we show a marginal increase in performance at best, the divergence of the 8mm optical configuration was much larger than that of the 50mm optical configuration.

The 50mm optical configuration resulted in a much more gradual decrease in signal providing a decay in signal of $1/d^{0.96}$. This is a significant improvement from the $1/d^2$ expectation when using focusing optics. Additionally, after approximately two meters, the decay appears nearly linear and constant. An excitation beam that is diverging to a lesser extent provides a decay profile that is significantly different and improved from the expected $1/d^2$ profile. This affords the user much greater flexibility in where and how they can use the instrument yet still obtain workable data up to meters away without changing any settings or optics. The relationship between divergence (i.e. degree of collimation) shown here is generally that as the divergence increases, the exponential decay of the signal will approach the theoretical $1/d^2$. Additional data (not reported here) also showed a similar test with a divergence 4.3mm/m resulting in an exponential fit of $1/d^{1.3}$, further validating this relationship.

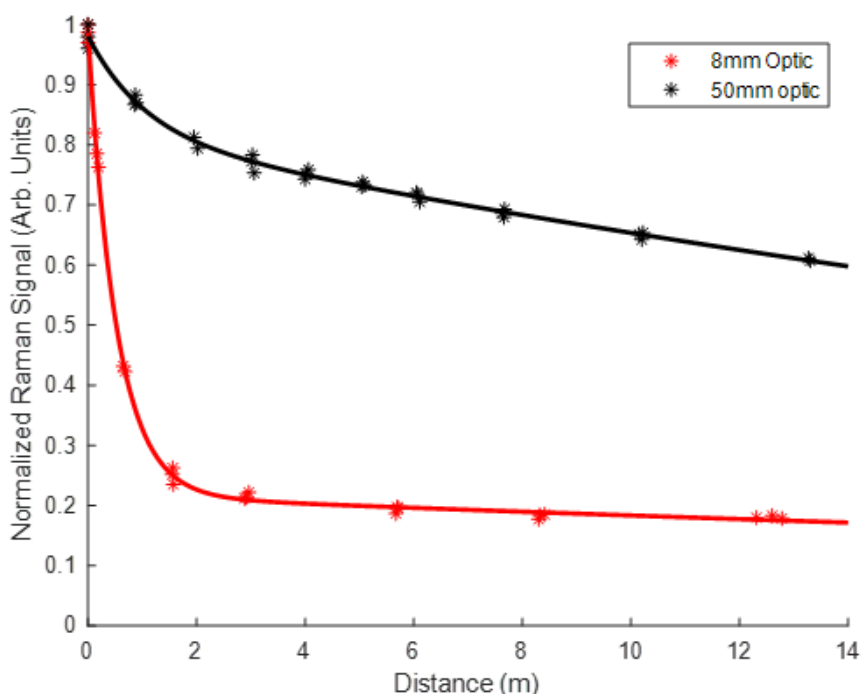


Figure 3: Normalized distance dependence of the Raman signal from ammonia nitrate with 8mm optics (red data) and 50mm optics (black data).

3.3 Understanding Parameters Effecting Distance-Dependence Signal Loss

However, despite the differences between these two beams, it can be measured and evaluated for influence on the decay profile of Raman signal. In fact, additional testing was completed to show the convolution of these factors. Here, two configurations using 8mm optics and 50mm optics were employed and the resulting excitation laser diameters were evaluated using naphthalene, shown in Figure 4. These configurations were slightly different than the data presented in Figure 2 as the top was opened on the instrument and optical arrangement was modified to better understand the parameters involved. The 8mm optical configuration have a divergence of 18.45 mm/m (diameter/divergence, blue data) and the 50mm optical configuration have a divergence of 3.7 mm/m (diameter/divergence, green data). When evaluating the distance dependence on Raman signal with these data, shown in Figure 5, the normalized Raman signal was shown to behave similarly between the optics as previously shown (Figure 3). The decay profiles of the 8mm optical configuration (blue data) are fit to a double exponential with the first exponential of $1/d^{1.69}$ and the second exponential of $1/d^{0.26}$. This is in stark contrast to the 50mm optical configuration (green data) that is well-fit to a single exponential of $1/d^{1.25}$. Understanding how the excitation and the acceptance angle of the spectrometer influence this can help provide insight into developing a more robust and less sensitive-to-distance instrument.

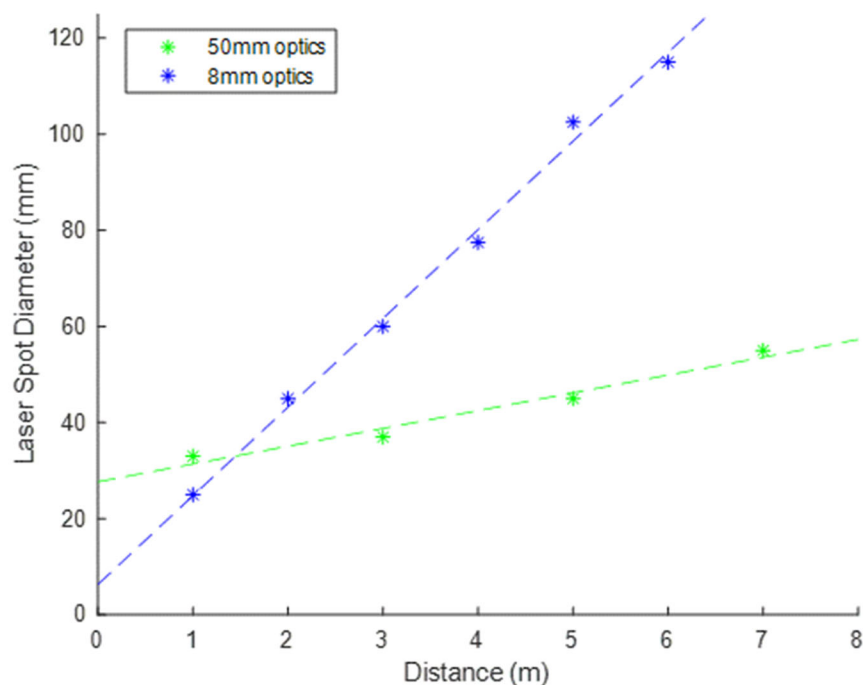


Figure 4: Excitation laser beam diameters as a function of distance with the 8mm optical configuration (blue data) and the 50mm optical configuration (green data).

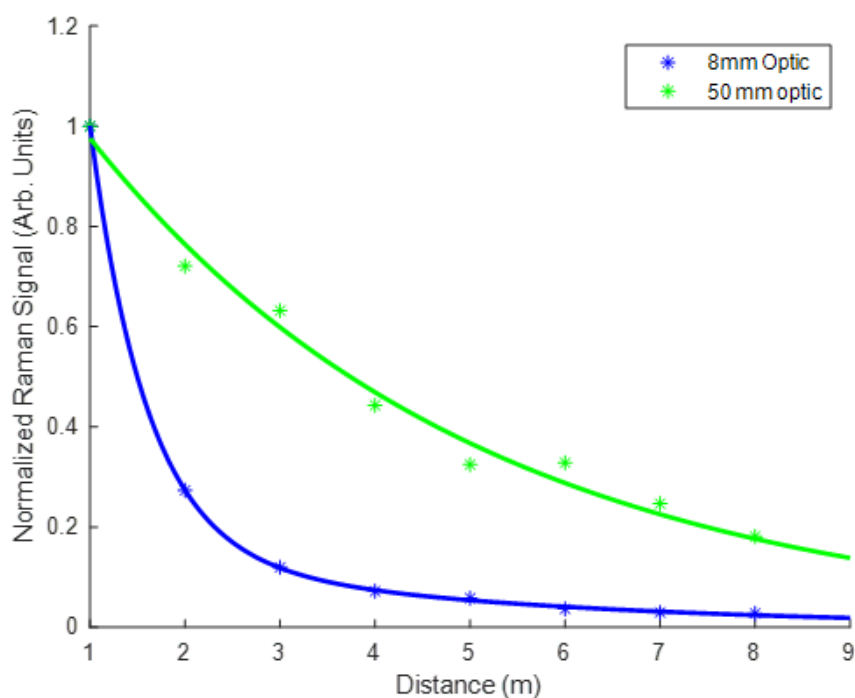


Figure 5: Distance dependence of Raman signal with modified configurations of 8mm optics (blue data) and 50mm optics (green data).

The results of the differences between the excitation and the acceptance cone diameter of the spectrometer for the 8mm optical configuration (blue data) and the 50mm optical configurations (green data) are shown in Figure 6. Here the

acceptance cone is a projection of the sample spot size that could be received in the collection optics based on the degree of collimation of the 8mm and 50mm optical configurations and the fiber coupling lens used to deliver the collected signal into the detector. The excitation and the acceptance cone diameters (open circles and asterisks, respectively) for the 8mm optical configuration are considerably different with slopes of 18.45mm/m and 4.25mm/m, respectively. The authors expect excitation beam and the acceptance cone diameter of the spectrometer profiles were different in the previous data (Figure 2 and Figure 3, red and black data) which is why the 18.45mm/m divergence results in a better-than-expected decay profile. If the excitation and acceptance cone diameters are better matched, the decay profile should be improved.

This finding validated with the 50mm optical configuration with the excitation beam and the acceptance cone diameter being matched with slopes of 3.7mm/m each (green data: open circles and asterisks, respectively). The double exponential can then be reduced to a single exponential and the two terms are no longer convoluting the signal response. Future work will be towards optimizing the internal collimating optics to provide overlapping excitation and acceptance cone diameters that are collimated. This, in theory, could provide line-of-sight limited Raman scatter collection as the signal decrease is expected to be minimal with completely collimated optics. This was shown previously with a laboratory-based instrument (not hand-held proximal) which showed less than 10% decay in signal over approximately 8m.⁸

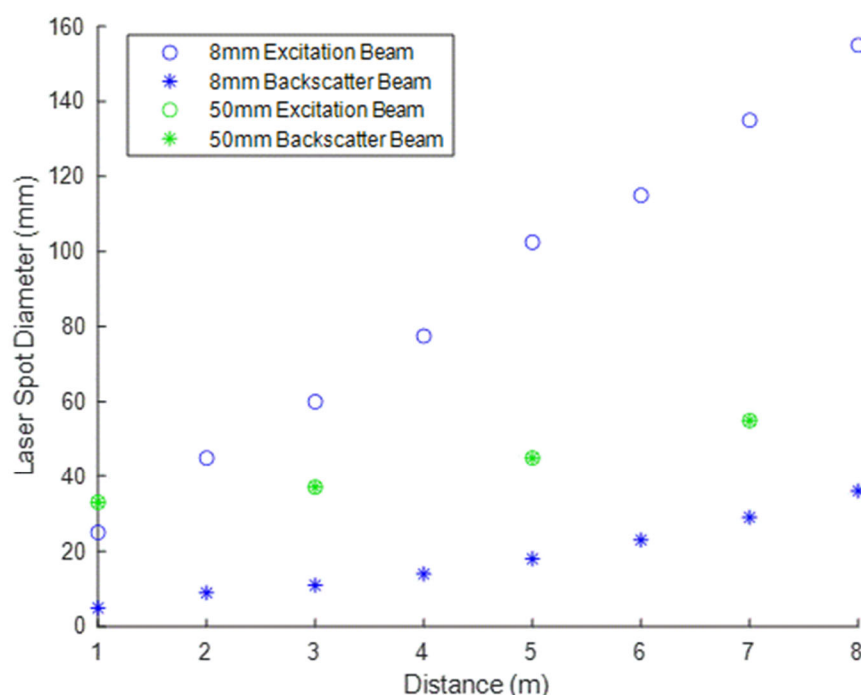


Figure 6: The beam profiles (diameters) of the 8mm excitation beam (blue open circles) and acceptance cone diameter (blue asterisks) compared to the 50mm optical configuration excitation beam (green open circles) and acceptance cone diameter (green asterisks).

3.4 Raman Imaging with Proximal Instrumentation

One potential application of using a proximal Raman detector that interrogates a larger surface (8mm vs 50mm optical configurations) is Raman imaging. In this portion of the study, ammonium nitrate was placed on a stainless steel coupon (2"x2") and the coupon was placed on an a translational stage with x- and y-axis translational capabilities. Three areas of analyte were placed on the stainless steel coupon, as shown in Figure 7. The various areas were used to highlight differences in detections with different interrogation areas. The blue and yellow highlighted areas have proportionally similar amounts of analytes. However, the red highlighted area has a much smaller amount of analyte distributed over a larger area, that is, it has a lower surface density.

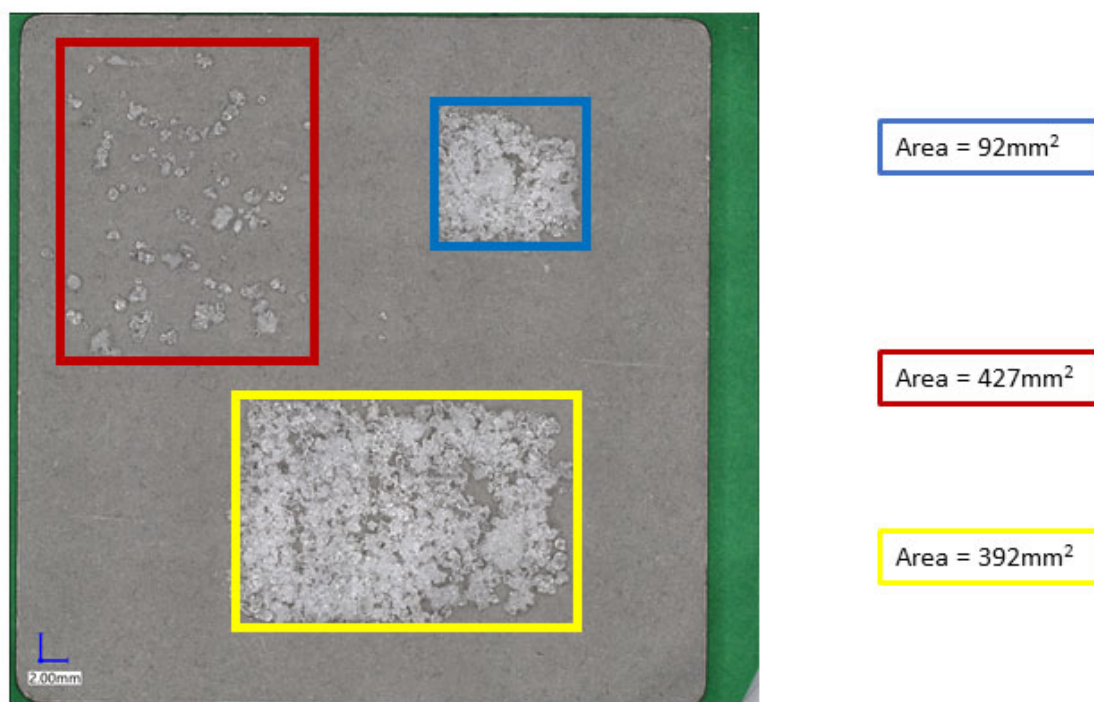


Figure 7: A 2" x 2" stainless steel coupon with three regions of ammonium nitrate placed on it with the smallest area highlighted in blue, the least analyte-dense area highlighted in red and the largest area of analyte highlighted in yellow.

The 8mm optical configuration was initially used at a distance of 0.16m from the surface. This resulted in a laser spot size for interrogation of approximately 3.6mm. The stage was raster scanned in 7mm increments across the area of interest. The results are shown in Figure 8. The scaled Raman image in Figure 8 (top left) shows the area that is imaged via the red-dashed box of the stainless steel coupon (Figure 8, top right). The Raman image clearly has two areas of increased signal from the larger and the smaller area of analyte with the larger surface density which correspond well with the digital image of the coupon. Additionally, pixels A, B, C, and D (Figure 8 top left and bottom middle) provide spectral confirmation of the ammonium nitrate (or none where it is not expected). In Figure 8 (bottom), the blue line is of Location A which is an area that has no ammonium nitrate and does not present a peak at 1041cm^{-1} . However, Locations B, C, and D, which correspond to the red, blue and yellow areas in Figure 7, respectively, show spectral responses similar to what would be expected. That is, Location B has the lowest spectral response at 1041cm^{-1} , which is expected as the surface density in that area is the lowest and the particles are most spread out (i.e. the least amount of analyte per interrogation area). Location C and D are similar in height as they are similar in surface density and provide a strong peak at 1041cm^{-1} . There are visual similarities between the color-scaled image and the digital image shown in Figure 8.

Similar to the 8mm optical configuration that was shown in Figure 8, the 50mm optical configuration was also used to complete a raster-scanned image of the same ammonium nitrate on stainless steel. Figure 9 (top) shows a color-scaled image of the 1041cm^{-1} ammonium nitrate peak and the associated spectra of similar locations in Figure 9 (bottom). The biggest difference here between the two color-scaled Raman images when comparing Figure 8 and Figure 9 is that the optical resolution decreases between the two. Specifically, the 50mm optical configuration provided a laser spot size of approximately 12.3mm, about 3.4 times larger diameter than that of the 8mm optical configuration. The resulting decrease in optical resolution is clear when comparing the two. However, in the spectral analysis in Figure 9 (bottom), while the signal is considerably smaller, the differences between Locations A, B, C, and D are still evident with no ammonium nitrate signal at Location A, very little ammonium nitrate signal at Location B, and approximately equal ammonium nitrate signal at Locations C and D. This corresponds with the surface density of ammonium nitrate shown in Figure 7.

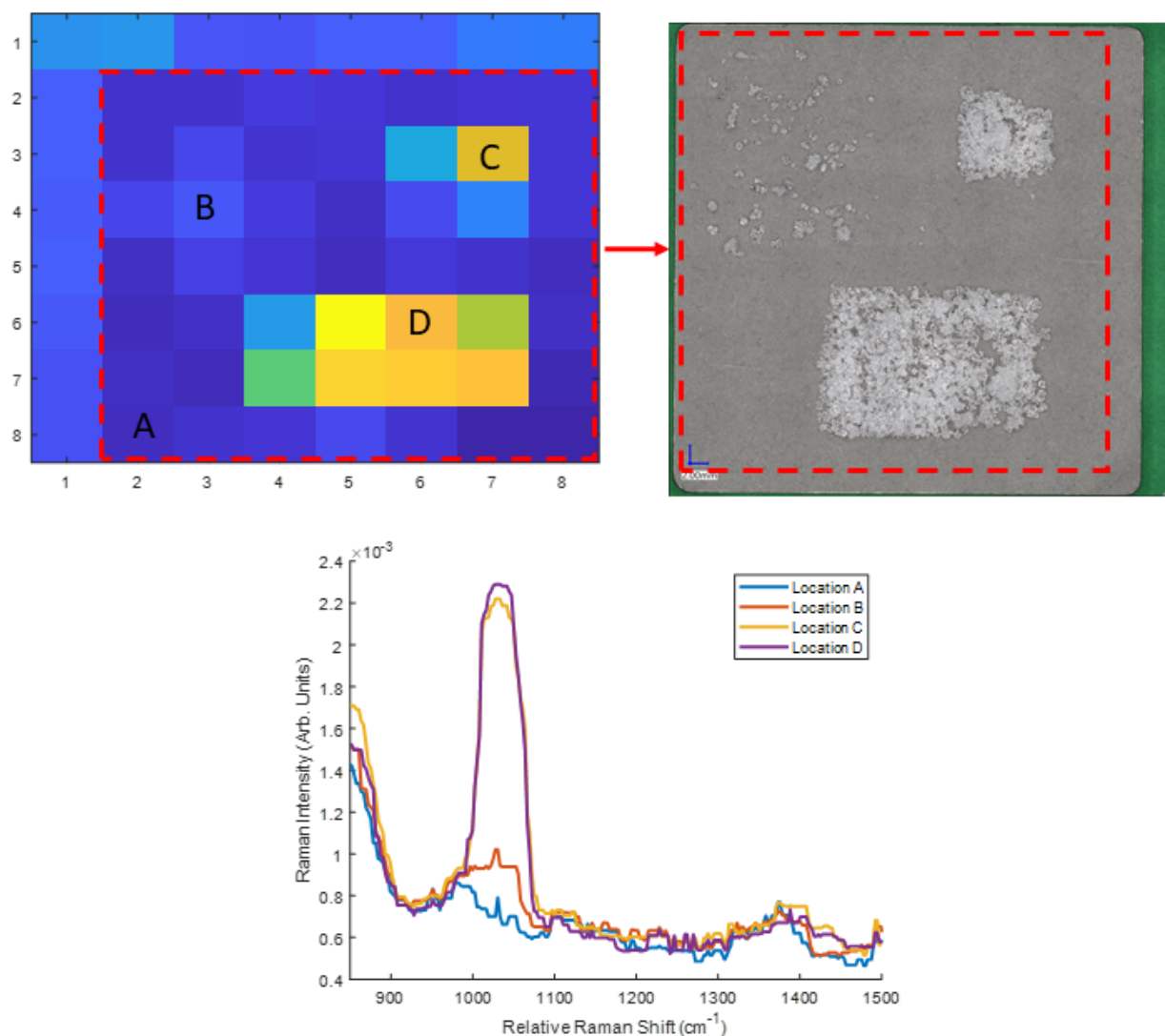


Figure 8: Raman image using the 8mm optical configuration (top left) of the stainless steel coupon (top right) with the imaging area highlighted in a red-dashed box. Spectra from spots A, B, C, and D are highlighted to show differences in which spot A is expected to have no analyte, Spot B is the low surface density area of analyte, and spots C and D are over the piles of ammonium nitrate with the peak at 1041cm^{-1} being analyzed for this image.

4. CONCLUSION

A handheld non-focusing based proximal Raman spectrometer shows promise for proximal and stand-off based explosives sensing. The decrease in Raman signal with respect to distance was found to range from $1/d^{1.9}$ to $1/d^{0.96}$, significantly improving upon the expected $1/d^2$ decay in signal with standard optics. Minimizing the amount of decay is realized when matching the excitation beam distance dependence with the acceptance cone from the detection spectrometer. Furthermore, Raman imaging can be realized using a non-focusing based proximal Raman spectrometer with the image resolution dependent on the interrogation area of the excitation beam. This work helps provide insight into what parameters to optimize to minimize distance-dependence signal loss when obtaining Raman spectra without focusing optics which increases a user's flexibility when assessing potentially dangerous compounds at a distance.

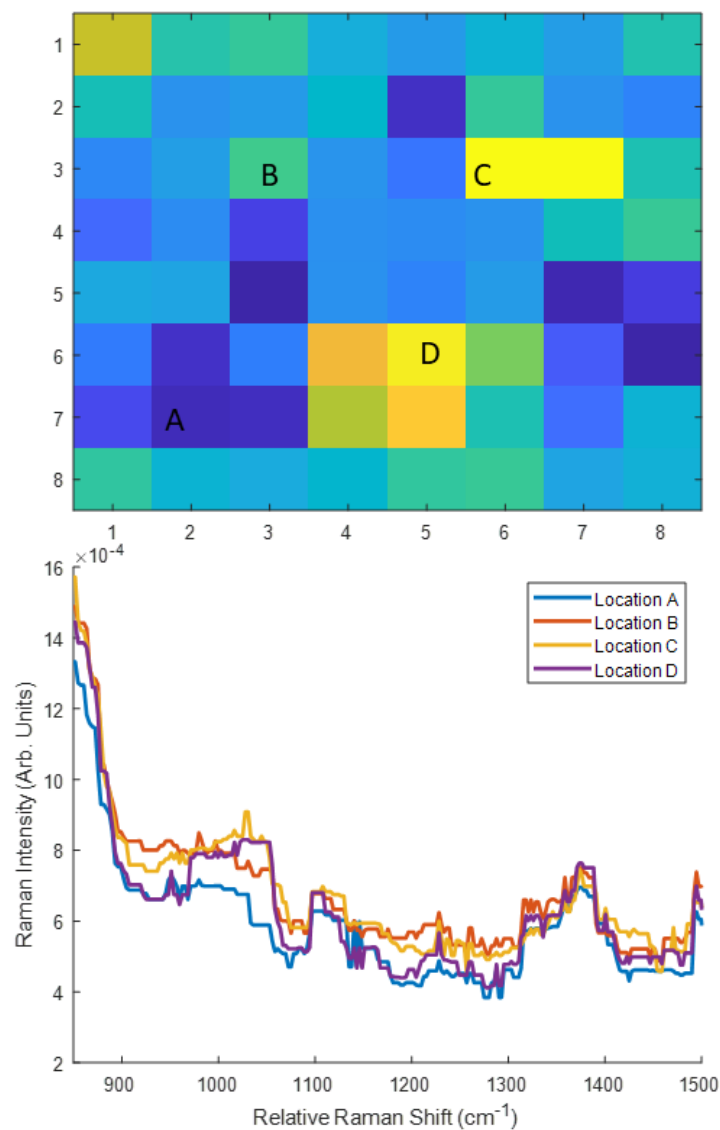


Figure 9: Raman image using the 25mm optical configuration (top) of the stainless steel coupon. Spectra from spots A, B, C, and D are highlighted to show differences in which spot A is expected to have no analyte, Spot B is the low surface density area of analyte, and spots C and D are over the piles of ammonium nitrate with a the peak at 1041cm^{-1} being analyzed for this image.

FUNDING

The work described in this report was authorized under the Army DEVCOM-CBC, Explosive Forensics program element number 0602144A and project number BL2.

REFERENCES

- [1] D. S. Moore, and R. J. Scharff, "Portable Raman explosives detection," *Analytical and Bioanalytical Chemistry*, 393(6), 1571-1578 (2009).
- [2] C. V. Raman, and K. S. Krishnan, "A New Type of Secondary Radiation," *Nature*, 121(3048), 501-502 (1928).
- [3] J. D. Ingle Jr, and S. R. Crouch, "Spectrochemical analysis," (1988).
- [4] R. Chirico, S. Almaguer, F. Colao *et al.*, "Proximal Detection of Traces of Energetic Materials with an Eye-Safe UV Raman Prototype Developed for Civil Applications," *Sensors*, 16(1), 8 (2016).
- [5] A. W. Fountain, S. D. Christesen, R. P. Moon *et al.*, "Recent advances and remaining challenges for the spectroscopic detection of explosive threats," *Applied spectroscopy*, 68(8), 795-811 (2014).
- [6] A. K. Misra, S. K. Sharma, T. E. Acosta *et al.*, "Single-Pulse Standoff Raman Detection of Chemicals from 120 m Distance during Daytime," *Applied Spectroscopy*, 66(11), 1279-1285 (2012).
- [7] J. Moros, J. A. Lorenzo, K. Novotný *et al.*, "Fundamentals of stand-off Raman scattering spectroscopy for explosive fingerprinting," *Journal of Raman Spectroscopy*, 44(1), 121-130 (2013).
- [8] B. R. Arnold, C. E. Cooper, M. R. Matróna *et al.*, "Stand-off deep-UV Raman spectroscopy," *Canadian Journal of Chemistry*, 96(7), 614-620 (2018).
- [9] J. Falk, "Measurement of laser beam divergence," *Applied Optics*, 22(8), 1131-1132 (1983).
- [10] Y. Suzuki, and A. Tachibana, "Measurement of the Gaussian laser beam divergence," *Applied Optics*, 16(6), 1481-1482 (1977).
- [11] N. Otsu, "A Threshold Selection Method from Gray-Level Histograms," *IEEE Transactions on Systems, Man, and Cybernetics*, 9(1), 62-66 (1979).
- [12] D. D. Tuschel, A. V. Mikhonin, B. E. Lemoff *et al.*, "Deep ultraviolet resonance Raman excitation enables explosives detection," *Applied spectroscopy*, 64(4), 425-432 (2010).
- [13] S. Elbasuney, and A. F. El-Sherif, "Instant detection and identification of concealed explosive-related compounds: Induced Stokes Raman versus infrared," *Forensic Science International*, 270, 83-90 (2017).